

# Supplemental Material: Kinetic phase diagram for nucleation and growth of competing crystal polymorphs in charged colloidal suspensions

Willem Gispen\* and Marjolein Dijkstra†

*Soft Condensed Matter, Debye Institute for Nanomaterials Science, Utrecht University*

## A. Code

The code to generate the results in this paper will be made publicly available in the Github repository [github.com/WillemGispen/kinetic-phase-diagram-charged-colloids](https://github.com/WillemGispen/kinetic-phase-diagram-charged-colloids). It is straightforward to repeat the calculations for other systems of interest. We use the LAMMPS molecular dynamics code [1].

## B. Molecular dynamics

We model a charge-stabilized colloidal suspension by a system where the electrostatic interactions between the colloids are described by a screened-Coulomb (Yukawa) potential

$$\beta u_Y(r) = \beta \epsilon \frac{\exp[-\kappa \sigma (r/\sigma - 1)]}{r/\sigma},$$

with  $\beta \epsilon$  the contact value and  $1/\kappa \sigma$  the Debye screening length. The excluded-volume interactions between the colloids are represented by a pseudo-hard-core potential

$$\beta u_{PHS}(r) = \frac{2C}{3} \left( \left( \frac{\sigma}{r} \right)^{50} - \left( \frac{\sigma}{r} \right)^{49} \right) + \frac{2}{3},$$

which reproduces well the hard-sphere equation of state using  $C = 134.6$  [2]. The total interaction potential of the pseudo-hard-core Yukawa system reads  $\beta u(r) = \beta u_Y(r) + \beta u_{PHS}(r)$ . Throughout this paper, we set  $\beta \epsilon = 81$ .

We perform molecular dynamics simulations by integrating Newton's equations of motion with the velocity-Verlet algorithm. The time step  $\Delta t^*$  that we used depends on the screening length  $1/\kappa \sigma$  as  $\Delta t^* = 0.02/\kappa \sigma$ . Here  $t^*$  refers to the reduced time unit  $t^* = t/\sqrt{\beta m \sigma^2}$  and  $m$  is the mass of a particle. The seeding simulations are carried out in the isobaric-isothermal ensemble, i.e. we keep the temperature  $T$  and pressure  $P$  fixed using a Nosé-Hoover thermostat and Nosé-Hoover barostat. The thermostat and barostat have a relaxation time of 100 and 500 time steps, respectively. The chemical potential simulations are carried out in the canonical ensemble, i.e. we keep the temperature  $T$  and volume  $V$  fixed. In addition, we use a cut-off distance of  $\sigma + 12/\kappa$  for the pair potential. At this cut-off distance, the pair potential has decreased to less than  $\beta u(r) = 10^{-5} \beta \epsilon$ .

## C. Free-energy calculations

We compute the chemical potential of a low-density ( $\rho \sigma^3 = 0.05$ ) fluid using Widom particle insertion method [3]. For the crystal phases, we use non-equilibrium Einstein integration [4] to determine the chemical potential at a high density (between  $\rho \sigma^3 = 0.3$  and  $\rho \sigma^3 = 0.6$ , depending on screening length). Subsequently, we calculate the chemical potential over the entire pressure range using thermodynamic integration of the equation of state

$$\mu(P) - \mu(P_0) = \int_{P_0}^P (1/\rho) dP.$$

To this end, we measure the equation of state using a step size of  $\Delta \rho \sigma^3 = 0.001$ . For each density and phase, we simulate about  $N = 4000$  particles for  $10^5$  simulation steps. We calculate the pressure using only the latter half of the simulation.

### 1. Spontaneous transformations

During the calculations of the equation of state, we check for spontaneous phase transformations. Most importantly, the bcc and fluid phase spontaneously transform at sufficiently high pressures. For the fluid phase, we monitor the largest crystal nucleus size as described in Section E2 of the SM. If the crystal nucleus comprises more than 5% of the system size, we identify it as spontaneous nucleation. In the case of bcc, we use polyhedral template matching (PTM) [5] with a root mean square deviation (RMSD) cutoff of 0.12. If more fcc or hcp particles are recognized by PTM than bcc, we identify it as a spontaneous transformation of bcc. In both cases, the lowest pressure at which the spontaneous phase transformation occurs is used to draw the boundaries in Fig. 1.

#### D. Comparison of the kinetic phase diagram with Ostwald step rule and the Alexander-McTague conjecture.

Using not only i) the equilibrium free energies of the fluid, fcc, and bcc phases, but also ii) the stability regimes of the fluid and bcc phase, as well as iii) the nucleation barrier heights of the two competing crystal phases for the entire metastable fluid regime, we can now compare directly the resulting kinetic phase diagram with Ostwald step rule and the Alexander-McTague conjecture. In Fig. S1, we first show the kinetic phase diagram according to Ostwald step rule, stating that the phase that is closest in free energy to the metastable fluid phase will nucleate first. This would result in a complete reversal of the bulk phase diagram, i.e. fcc nucleates when bcc is stable, and bcc nucleates when fcc is stable except in a small region close to the binodal where fcc or bcc is even less stable than the fluid phase, as is illustrated by the free-energy curves for the fluid, fcc, and bcc phase for  $1/\kappa\sigma = 0.3$  and  $0.125$  in Fig. S2.

The following picture emerges concerning the validity regimes of these rules. We find that Ostwald's step rule is only obeyed in the regime where metastable bcc nucleates. The Alexander-McTague conjecture is only obeyed where bcc is stable, because fcc nucleation is preferred near the fluid-fcc binodal. Hence, we do not expect to observe nucleation of bcc at low supersaturations in the case of weakly first-order freezing transitions as conjectured by Alexander and McTague.

We can rationalize these violations as follows. Firstly, our stability analysis reveals an extended region near the hard-sphere limit where the bcc phase becomes mechanically unstable. Therefore, bcc cannot form in this region, making the Alexander-McTague conjecture invalid here. Secondly, between the fluid-fcc binodal and the metastable fluid-bcc binodal, bcc cannot nucleate, as the free energy of the bcc phase is higher than that of the fluid phase. Thirdly, close to the metastable fluid-bcc binodal, the driving force for bcc nucleation  $|\Delta\mu_{bcc}|$  is extremely small. Since the nucleation barrier  $\Delta G \propto 1/|\Delta\mu|^2$  is inversely proportional to the square of the supersaturation  $|\Delta\mu|$ , the bcc nucleation barrier blows up near the metastable fluid-bcc binodal. Therefore, in this region the nucleation barrier is necessarily larger for bcc than for fcc.

So limitations of the Ostwald step rule and the Alexander-McTague conjecture can already be found by calculating the equilibrium free energies and the stability regimes of the competing phases. However, in order to determine the precise nucleation mechanism, one has to calculate and compare the nucleation barriers of the respective polymorphs at the state points of interest.

#### E. Seeding

##### 1. Seed preparation

For each phase and screening length, we prepare around 16 seeds with sizes varying between 100 and  $13 \times 10^3$  particles. We use seeds with at least 400 particles in order to calculate the nucleation barriers, and we employ all seeds for studying crystal growth. For a target seed size  $N$ , we simulate a supersaturated fluid phase and a crystal phase at the same pressure  $P$ . Subsequently, we cut a spherical region of approximately  $0.8N$  particles from the crystal and insert it into the fluid, such that the total system size is around twenty times as large as the target seed size. We keep the positions of the seed particles fixed and simulate the fluid for at most 8000 MD steps or until the largest crystal cluster in the system reaches the target size  $N$ . We then simulate the whole system for 4000 MD steps. If this procedure does not result in a crystal cluster within a size range of  $0.9 - 1.1N$  particles, we use a higher or lower pressure.

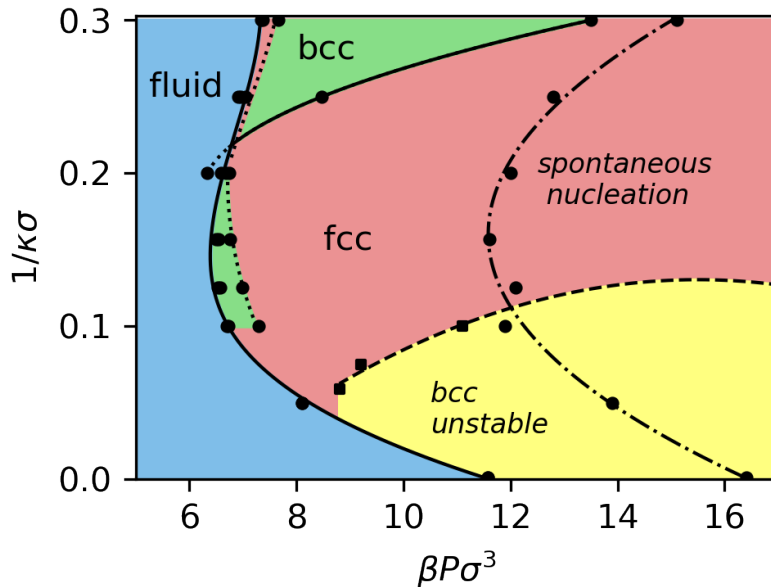


FIG. S1. Kinetic phase diagram according to Ostwald's step rule. The labels fluid, bcc, fcc denote the stable fluid, bcc, fcc region. The yellow region and the dashed line denote the region where bcc is unstable as it spontaneously transforms to fcc/hcp. The dashed-dotted line denotes the pressure above which spontaneous nucleation occurs. The red and green regions denote the regions where according to Ostwald's step rule bcc and fcc, respectively, should nucleate first.

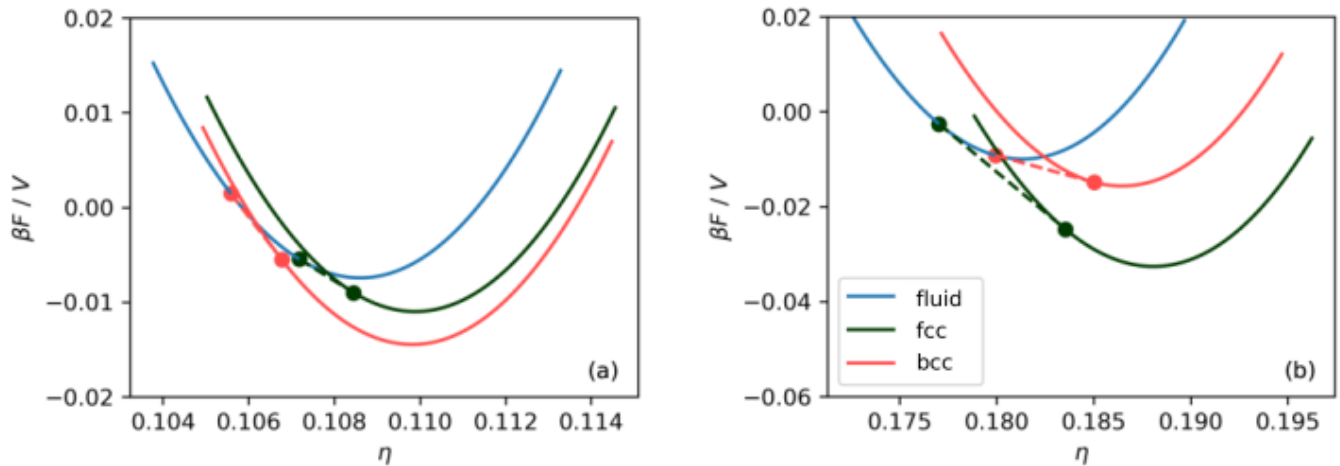


FIG. S2. Helmholtz free-energy density  $\beta F/V$  for a fluid, fcc, and bcc phase of highly charged colloids with  $\beta \epsilon = 81$  and (a)  $1/\kappa \sigma = 0.3$  and (b)  $1/\kappa \sigma = 0.125$  as a function of packing fraction  $\eta = \pi \sigma^3 N/6V$ . The dashed lines denote the common-tangent construction connecting the coexisting bulk phases.

## 2. Crystal nucleus size

To determine the crystal nucleus size, we use the mislabeling criterion [6] based on the locally averaged bond order parameter  $\bar{q}_6$  [7, 8].

To compute  $\bar{q}_6$ , we first detect the nearest neighbors  $N(i)$  of particle  $i$  with the solid-angle based, nearest-neighbour algorithm [9]. Next, the local density is projected on spherical harmonics

$$q_{lm}(i) = \frac{1}{N(i)} \sum_{j=1}^{N(i)} Y_{lm}(\mathbf{r}_j - \mathbf{r}_i).$$

These  $q_{lm}(i)$ 's are averaged over the nearest neighbors of  $i$  to obtain

$$\bar{q}_{lm}(i) = \frac{1}{1 + N(i)} \left( q_{lm}(i) + \sum_{j=1}^{N(i)} q_{lm}(j) \right).$$

Finally, the averaged bond order parameter is calculated with

$$\bar{q}_l(i) = \sqrt{\frac{4\pi}{2l+1} \sum_m |\bar{q}_{lm}(i)|^2}$$

The averaged bond order parameters  $\bar{q}_6(i)$ 's are calculated for each particle  $i$  in a bulk fluid and a bulk crystal, for a range of pressures. At each pressure, the mislabeling threshold  $\bar{q}_6^*$  is determined such that the percentage of bulk solid being mislabeled as fluid is equal to the percentage of bulk fluid being mislabeled as solid, i.e.

$$P(\bar{q}_6(i) > \bar{q}_6^* \text{ with } i \text{ fluid}) = P(\bar{q}_6(j) < \bar{q}_6^* \text{ with } j \text{ solid})$$

This mislabeling threshold  $\bar{q}_6^*$  then provides a local solid-fluid classification: particles with  $\bar{q}_6 > \bar{q}_6^*$  are solid-like, and particles with  $\bar{q}_6 < \bar{q}_6^*$  are fluid-like. The largest cluster of solid-like particles is found with a cut-off distance equal to the pair potential cut-off.

### 3. Active learning for determining the critical pressure and critical nucleus size from seeding simulations

To determine the critical pressure and critical nucleus size from seeding simulations, we use active learning and logistic regression. This procedure is based on the bisection method and logistic regression, taking care of stochasticity. For a fixed temperature, we first determine the interval in which the critical pressure  $P^*$  lies. Subsequently, we repeat the following three steps:

1. Estimate the critical pressure, say  $P_{\text{est}}^*$ , with logistic regression.
2. Simulate the seed at the estimated pressure  $P_{\text{est}}^*$  for at most  $10^5$  MD steps or until it grows to 30% or melts to 0.5% of the system size.
3. Add  $(P_{\text{est}}^*, B)$  to the list of observations, where  $B \in \{0, 1\}$  indicates whether a seed grew or melted.

In the first step, the estimated critical pressure is simply the pressure for which the regression estimates a 50% probability of growth. Simulating at this estimated critical pressure corresponds to the so-called 'uncertainty sampling' approach to active learning [10]. Using logistic regression in this way circumvents the need to estimate the crystallization probability at a single pressure using multiple runs. The final estimate for the critical pressure is obtained after fitting 50 observations obtained in the way just described.

### 4. Classical nucleation theory

We fit the obtained nucleation barriers using classical nucleation theory (CNT). From the critical nucleus size  $N^*$  and the supersaturation  $|\Delta\mu(P^*)|$  at the critical pressure  $P^*$ , we approximate the surface tension  $\gamma(P^*)$  with the CNT expression

$$\gamma^3 = \frac{3N^*|\Delta\mu|^3\rho^2}{32\pi}.$$

Here  $\rho$  is the density of the crystal phase at critical pressure  $P^*$ . Next, we fit the surface tension linearly as a function of pressure, and estimate the error of this fit using Ref. [11]. Finally, this leads to the CNT fit

$$\Delta G = \frac{16\pi\gamma^3}{3|\Delta\mu|^2\rho^2},$$

which can be extrapolated to the entire metastable fluid region. The error in  $\Delta G$  is estimated from the error in  $\gamma$ , where we neglect the errors in  $\Delta\mu$  and  $\rho$ .

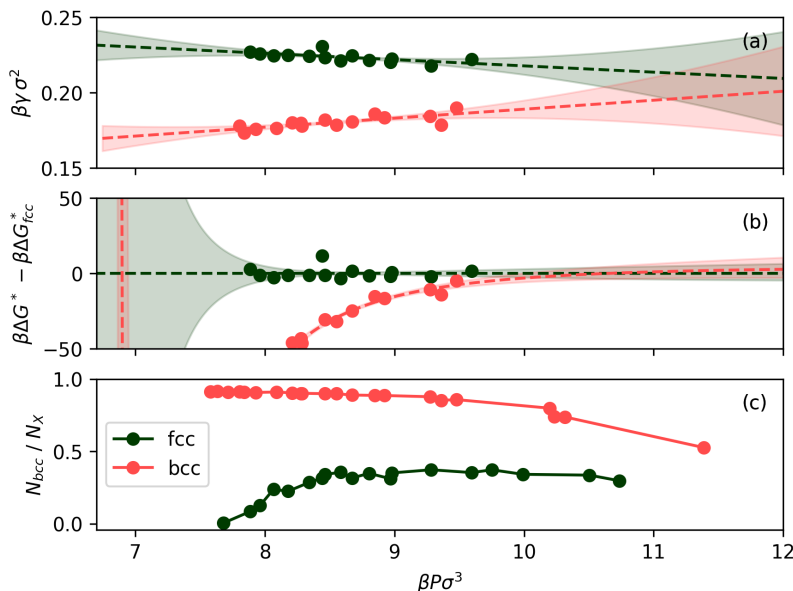


FIG. S3. Results as obtained from seeding simulations of a suspension of highly charged colloids with a contact value  $\beta\epsilon = 81$  and a Debye screening length  $1/\kappa\sigma = 0.2$ . The dashed lines denote the fits using classical nucleation theory and the shaded areas denote the estimated error of the fits. (a) The solid-fluid surface tension  $\gamma$  as a function of pressure  $\beta P\sigma^3$ , (b) difference in nucleation barrier with respect to fcc,  $\Delta G^* - \Delta G_{fcc}^*$ , as a function of pressure  $\beta P\sigma^3$ , and (c) fraction of bcc-like particles  $N_{bcc}/N_x$  in the crystal growth of fcc and bcc seeds as a function of pressure  $\beta P\sigma^3$  where  $N_{bcc}$ ,  $N_{fcc}$ , and  $N_{hcp}$  refer to the number of bcc, fcc, and hcp particles, respectively, as recognized by polyhedral template matching, and  $N_X = N_{fcc} + N_{bcc} + N_{hcp}$  is the total number of crystalline particles. The nucleation barrier difference in (b) becomes smaller than the estimated error for  $\beta P\sigma^3 > 10$ .

### 5. Seeding simulation results for charged colloids with $1/\kappa\sigma = 0.2$

Exemplarily, we show seeding simulation results for a suspension of highly charged colloids with a contact value of  $\beta\epsilon = 81$  and screening length  $1/\kappa\sigma = 0.2$ , which is close to the triple point. In Fig. 2, we plot the critical nucleus size  $N^*$ , the supersaturation  $\Delta\mu$  and the nucleation barrier  $\Delta G^*$ . In Fig. S3, we show the fluid-solid surface tension  $\gamma$ , the difference in nucleation barrier  $\Delta G^* - \Delta G_{fcc}^*$ , as well as the fraction of bcc in the crystal growth of bcc and fcc seeds. In this region, the bcc phase is metastable with respect to fcc, as can be seen from the lower chemical potential for fcc with respect to bcc in Fig. 2c. However, Fig. S3a shows that bcc has a lower interfacial tension with the fluid phase than fcc. This lower surface tension causes the nucleation barrier of bcc to be lower in the pressure range  $6.9 < \beta P\sigma^3 < 10.1$ . For these pressures, the bcc seeds grow out to pure bcc crystals, whereas fcc seeds grow out into a mix of fcc, hcp and bcc (see Fig. S3c of the SM). At  $\beta P\sigma^3 = 10$ , the nucleation barrier difference as shown in Fig. S3b becomes smaller than the estimated error. Above this pressure, the fraction of bcc in the crystal growth of bcc seeds decreases rapidly. The same trend is also observed for the other screening lengths: the pressure beyond which the nucleation barriers become indistinguishable, the ‘purity’ of the seeds decreases rapidly.

## F. Phase diagrams in the packing fraction - Debye screening length plane

In Fig. S4, we show the bulk phase diagram in the packing fraction - Debye screening length plane, in contrast to the pressure - Debye screening length plane shown in the main text. In this presentation, we can see that spontaneous nucleation occurs for packing fractions only 2 – 3% above the fluid-solid binodal. The fcc-bcc coexistence region is extremely narrow, in fact it is smaller than the linewidth used in the plot.

In Fig. S5, we also show the kinetic phase diagram in the packing fraction - Debye screening length plane. Only for packing fractions less than 2% above the fluid-solid binodal, we observe (relatively) pure crystals, ranging from fcc/hcp, to metastable bcc, to bcc, upon increasing  $1/\kappa\sigma$ . Therefore, pure metastable bcc can only form in a narrow region near the triple point and near the fluid-solid binodal. For higher packing fractions, we find a mix of fcc, hcp and bcc crystal grains. In contrast to the extremely narrow stable fcc-bcc coexistence in Fig. S4, this non-equilibrium

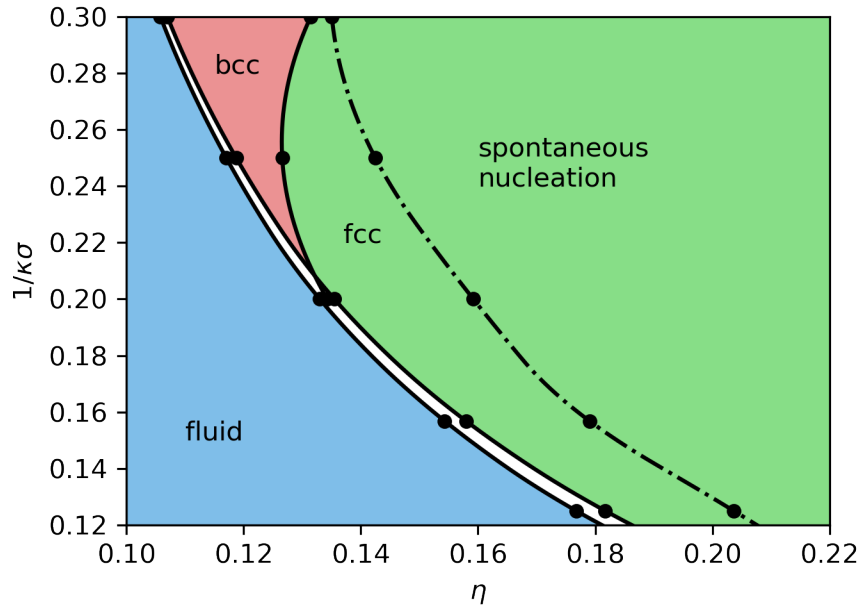


FIG. S4. Bulk phase diagram of highly charged colloids with contact value  $\beta\epsilon = 81$  in the packing fraction  $\eta$  - Debye screening length  $1/\kappa\sigma$  plane. The fluid-solid and bcc-fcc binodals are denoted by solid lines, and the dash-dotted line marks the pressure beyond which the fluid spontaneously crystallizes. Dots are the actual measurements, lines are spline interpolations to guide the eye.

mix of fcc/hcp and bcc forms in a broad region of the phase diagram.

\* w.h.gispen2@uu.nl

† m.dijkstra@uu.nl

- [1] S. Plimpton, *J. Chem. Phys.* **117**, 1 (1995).
- [2] J. Jover, A. J. Haslam, A. Galindo, G. Jackson, and E. A. Müller, *J. Chem. Phys.* **137**, 144505 (2012).
- [3] B. Widom, *J. Chem. Phys.* **39**, 2808 (2004).
- [4] R. Freitas, M. Asta, and M. de Koning, *Comput. Mater. Sci.* **112**, 333 (2016).
- [5] P. M. Larsen, S. Schmidt, and J. Schiøtz, *Modelling Simul. Mater. Sci. Eng.* **24**, 055007 (2016).
- [6] J. R. Espinosa, C. Vega, C. Valeriani, and E. Sanz, *J. Chem. Phys.* **144**, 034501 (2016).
- [7] P. J. Steinhardt, D. R. Nelson, and M. Ronchetti, *Phys. Rev. B* **28**, 784 (1983).
- [8] W. Lechner and C. Dellago, *J. Chem. Phys.* **129**, 114707 (2008).
- [9] J. A. van Meel, L. Filion, C. Valeriani, and D. Frenkel, *J. Chem. Phys.* **136**, 234107 (2012).
- [10] B. Settles, *Active Learning Literature Survey*, Computer Sciences Technical Report 1648 (University of Wisconsin–Madison, 2009).
- [11] P. H. Richter, *TDAPR* **122**, 107 (1995).

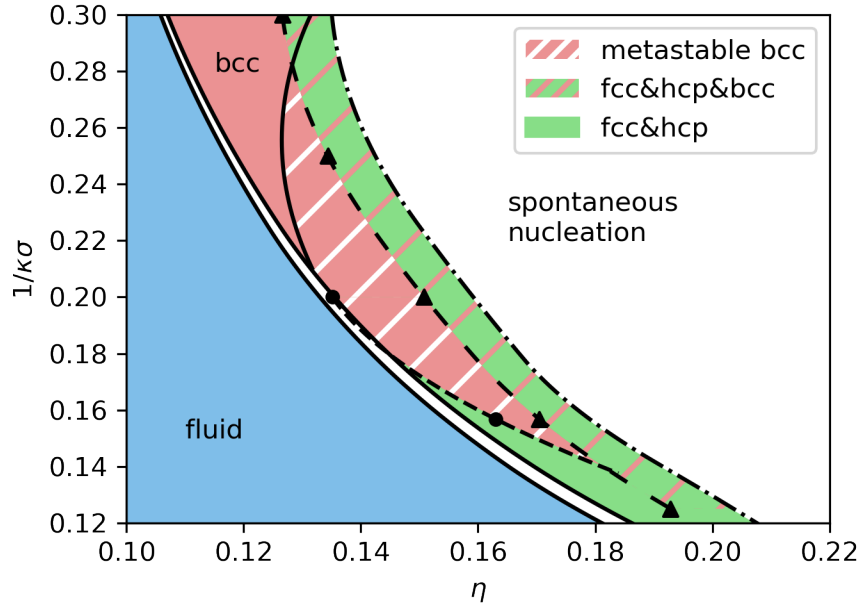


FIG. S5. Kinetic phase diagram of highly charged colloids with contact value  $\beta\epsilon = 81$  in the packing fraction  $\eta$  - Debye screening length  $1/\kappa\sigma$  plane. The fluid-solid and fcc-bcc binodals are denoted by solid lines, and the dash-dotted line marks the pressure beyond which the fluid spontaneously crystallizes. The red (green) region denotes the region where bcc (fcc) has a lower nucleation barrier than fcc (bcc). The red region with stripes near the triple point denotes the metastable bcc region, where bcc has a lower nucleation barrier while being metastable. The triangles mark the pressures above which the nucleation barriers of fcc and bcc are indistinguishable within our statistical accuracy. Dots are actual measurements and lines are spline interpolations to guide the eye.